JMEPEG (1992) 1:547-554

Isothermal and Thermomechanical Finite-Element Analysis of the Tube Drawing Process Using a Fixed Tapered Plug

J. Rasty and D. Chapman

Quality is a very important feature in the manufacturing of products such as tube. Nonhomogeneous deformation, common to most metalforming operations, leaves the product in a cold worked state, resulting in a pattern of residual stresses. Depending on the nature and magnitude of residual stresses, they may be detrimental or beneficial to the strength and reliability of the product. To evaluate the residual stresses in the product, a complete stress analysis of the workpiece throughout the deformation history is required. In this study, a large deformation, nonlinear, elastic-plastic finite-element code was used to investigate the effect of friction, drawing speed, degree of plastic work (reduction in area), and the die/plug geometry on the extent of temperature increase, induced residual stresses, and the required drawing load in the drawing of oxygen-free high-conductivity (OFHC) copper tube using a fixed, tapered plug. Complete simulations of the tube drawing process were conducted by tracing its deformation history from the point at which it entered the die area until it exited the die. The resulting thermal effects were then used to determine the required drawing loads and induced residual stress distributions throughout the tube wall thickness. Similar simulations were conducted without taking into account the thermal effects. Equivalent plastic strain, equivalent stress, longitudinal stress, and circumferential residual stresses are presented and compared for both the isothermal and the thermally coupled analysis.

1. Introduction

IN the metalforming industry, the drawing of tube is a process in which a tube is pulled through a conical converging die, reducing both the diameter and the tube thickness. The various types of plugs used in tube drawing are fixed tapered plugs, floating plugs, moving plugs, and cylindrical plugs. In tube drawing with a fixed tapered plug, a stationary tapered plug is used to reduce the outer and inner radius as well as a reduction in wall thickness. A complete literature survey is available in Chapman.[1]

The goal in most manufacturing processes is to produce the highest quality product at the lowest price. Metalforming processes commonly generate nonhomogeneous deformation in the workpiece, so that the final product is left in a work-hardened state containing a pattern of residual stresses. Residual stresses are self-equilibrating internal stresses that exist in a free body in the absence of external forces. The nature and distribution of residual stresses affect fatigue behavior, stress-corrosion characteristics, and dimensional stability during machining. Residual stresses are either detrimental or beneficial to the quality of the product. If a workpiece is to be machined, removal of the stressed material leads to residual deformation, which increases with increasing stress magnitudes.

The fatigue strength of metals is greater when the residual stress on the outer surface is compressive rather than tensile. Residual compressive stresses on the surface effectively reduce the tensile stresses to a level that does not cause cracking or failure. Residual tensile stresses significantly increase the effective stress levels and lead to unanticipated fractures. Drawing stress is the longitudinal stress in the tube wall at the exit of the die and plug. It is the force required to pull the tube through the die and plug divided by the cross-sectional area of the drawn tube.

The methods of determining drawing stress and residual stresses are experimental, analytical, or numerical. The experimental methods are very costly and time consuming. Analytical methods can be used to determine drawing stress; however, residual stresses cannot be determined. Drawing stresses and residual stresses can be determined from a numerical analysis, such as the finite-element method. Finite-element analysis is a structural analysis technique that uses the computer to simulate the response of a specimen to a variety of loadings and environmental conditions.

In many metalforming operations, heat is produced by the plastic deformation and work required to overcome friction. This heat causes a change in temperature, which can influence the material properties and generate thermal strains. A thermal analysis is performed by superimposing or coupling the mechanical and thermal deformations.

This study was performed with die angles of 15.0, 17.5, 20.0, and 22.5°. The plug angles were varied 2.5, 5.0, and 7.5° less than the die angles. Reductions in area of 10.9 and 37.1% were also incorporated into the simulations. These reductions in area correspond to tempers of quarter-hard and hard, respectively. The drawn material was oxygen-free high-conductivity (OFHC) copper.

2. Finite-Element Analysis

The finite-element method has evolved over the past 25 years from a specialized technique for aircraft frame analysis to

J. Rasty, Assistant Professor, Department of Mechanical Engineering, Texas Tech University, and **D. Chapman**, Graduate Student, Texas Tech University, Lubbock, Texas.

a general numerical solution technique applicable to a broad range of physical problems of complex geometries composed of materials that exhibit nonlinear behavior. The approach used in the analysis of the tube drawing operation consisted of using a finite-element code that was capable of modeling linear and nonlinear problems involving the large deformations encountered in metalforming processes.

The basic concept behind the finite-element code is the subdivision of a region into sufficiently smaller regions or elements, so that the solution can be represented by a mathematical function. The regions or elements are connected at points called nodes. Assumed displacement functions are used to approximate the actual displacement within each element. The principle of virtual work is used to obtain the equations of equilibrium from the shape functions. The equilibrium equations for the entire model are combined so that the continuity of displacements at the nodes is preserved. The boundary conditions are added to the model, and the model is solved for the displacements. From these displacements, the strains and stresses are calculated.

To analyze a given problem, the initial configuration is first described, and the deformation is sought throughout the history of loading. A particle is initially located at position X and moves to a new location x. Assuming conservation of mass, the history of the location of the particle is written as:

$$x = x(X,t) \quad [1]$$

where t is time. Consider two neighboring particles located at X and at $X + dX$ in the initial configuration, dX is the infinitesimal length. The initial infinitesimal length is

$$dL^2 = dX^T \cdot dX \quad [2]$$

and the final infinitesimal length can be written as:

$$dl^2 = dx^T \cdot dx \quad [3]$$

The stretch length is defined as:

$$\lambda = \frac{dl}{dL} = \sqrt{\frac{dx^T \cdot dx}{dX^T \cdot dX}} \quad [4]$$

If $\lambda = 1$, there is no strain of this infinitesimal gauge length, but rigid body motion is possible. The true strain is found from the stretch length by:

$$\varepsilon = \ln \lambda \quad [5]$$

For problems with large discontinuities, such as plasticity analysis with large strains, first-order fully integrated elements are recommended.[2] This agrees with the findings of Kopp and Chu,[3] who studied different element types and recommended the four-node axisymmetric element. Four-node axisymmetric quadrilateral elements were used in the isothermal model of the copper tube. Coupled four-node axisymmetric quadrilateral elements were used in the coupled temperature-displacement analysis. The coupled temperature-displacement elements were fully coupled heat transfer and stress analysis elements.

The finite-element code used in this study has the ability to model linear and nonlinear material properties. Constitutive equations are mathematical models describing, for a given material, the relations between deformation, strain, and stress. The elastic-plastic material was modeled using the incremental plasticity theory. A rate-dependent material model was used. Deformation in an elastic-plastic material is divided into an elastic part and a plastic part. This statement is written as:

$$F = F^{el} + F^{pl} \quad [6]$$

where F is the total deformation, F^{el} is the elastic deformation, and F^{pl} is the plastic deformation. The strain is obtained directly from the deformation and is used to formulate the plasticity model:

$$\varepsilon = \varepsilon^{el} + \varepsilon^{pl} \quad [7]$$

Here, ε is total strain, ε^{el} is the elastic strain, ε^{pl} is the plastic strain. The elastic stress is defined by:

$$\sigma = E\varepsilon^{el} \quad [8]$$

The limit to the elastic region is defined by the von Mises yield function given by:

$$f(\sigma) = \frac{\sqrt{\left(\sigma_r - \sigma_\theta\right)^2 + \left(\sigma_z - \sigma_\theta\right)^2 + \left(\sigma_r - \sigma_z\right)^2}}{2} + 3\sigma_{rz}^2 \quad [9]$$

The plastic part of the response is described by the incremental plasticity theory as:

$$d\varepsilon^{pl} = d\lambda \frac{\partial f}{\partial \sigma} \quad [10]$$

where $d\lambda$ is a constant. The previous equation can be rewritten as:

$$\Delta\varepsilon^{pl} = \Delta\lambda \frac{\partial f}{\partial \sigma} \quad [11]$$

This equation is then numerically integrated over time.

3. Simulation Parameters

Because tube drawing is inherently axisymmetric, the use of axisymmetric elements means that the geometry of the model is simplified. Four-node axisymmetric quadratic elements were used to model the tube for the isothermal case, and four-node fully coupled axisymmetric elements were used to model the coupled case. The die and plug are rigid surfaces and contact interface elements. A smoothing option was used to smooth the sharp corners on the rigid surfaces. A coefficient of friction of 0.05 was used.

The final dimensions of the tube are assumed, and the initial diameters are calculated from the die and plug angles, reduc-

tion in area, and the following relationship between the initial and final inside and outside radii.

$$\frac{R_{of}}{R_{if}} = \frac{R_{oi}}{R_{ii}} \qquad [12]$$

The reduction in area is given by:

$$\%\Delta R = 100\left[1 - \left(\frac{R_{of}^2 - R_{if}^2}{R_{oi}^2 - R_{ii}^2}\right)\right] \qquad [13]$$

A mesh study was conducted to determine the aspect ratio of the elements, the density of the mesh, and the length of the tube model. The aspect ratio is the ratio of the length to the width of each element. To determine the optimum aspect ratio, the tube drawing process was simulated with ratios of 1:1, 1.5:1, 2:1, and 3:1. The aspect ratio of 2:1 was determined to be suitable.

The optimum mesh density was determined by simulating the tube drawing process with four, six, eight, and twelve elements in the radial direction. The solution varied little with the number of elements in the radial direction; however, sufficient data are needed to obtain an accurate view of the stress distribution in the cross section. Six elements in the radial direction were chosen.

The length of the tube model was studied to determine the required length of the workpiece. The tube drawing process was simulated with different lengths to study the effect of length. The minimum required length of tube was found to be no shorter than 1.5 times longer than the length of the die.

The stiffness in stick, G, is defined[4] as the average pressure on the surface of an element times the coefficient of friction divided by the average distance of slip in the increment. This is written as:

$$G = \frac{P_\mu}{l} \qquad [14]$$

The amount of slipping in an increment is dependent on the size of an increment, the geometry of the problem, and the rate of convergence.

Because of the ambiguity of the stiffness in stick parameter, a study was performed to determine the effect of the stiffness in stick parameter on tube drawing simulations. An axisymmetric compression test was modeled (Fig. 1) to test the stiffness in stick parameter. Only the upper fourth was modeled due to the symmetry in the radial and axial directions.

Figure 2 shows the deformation patterns and how they vary with the stiffness in stick parameter. When a small value is used for the stiffness in stick parameter, homogeneous deformation results. As the stiffness in stick increases, the amount of nonhomogeneous deformation increases. In Fig. 3, the maximum val-

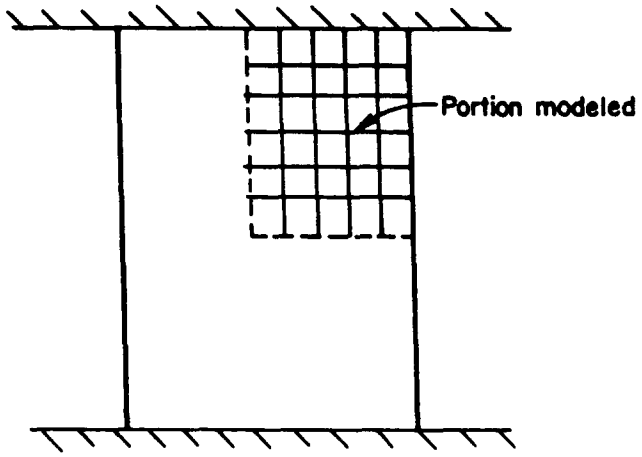

Fig. 1 Schematic of axisymmetric compression test.

Table 1 Results of Stiffness in Stick Study

Stiffness, N/m	σ_r, MPa	σ_z, MPa	σ_θ, MPa	$\sigma_{r\theta}$, MPa	σ_e, MPa	Load, kN
1.0.....	–0.1	–349.6	–0.1	0.0	349.4	2,818
100.0.....	–6.5	–355.9	–6.5	–1.2	349.4	2,836
1000.0.....	–63.3	–412.4	–62.6	–11.8	349.4	2,934
2000.0.....	–214.6	–516.6	–209.8	–30.1	349.4	3,031
5000.0.....	–277.3	–623.1	–270.9	–54.8	349.4	3,191
10,000.0....	–504.0	–811.8	–459.5	–64.7	349.4	3,182
50,000.0....	–430.5	–767.1	–417.1	–70.5	349.4	3,122
70,000.0....	–445.8	–762.4	–412.0	–70.5	349.4	3,133

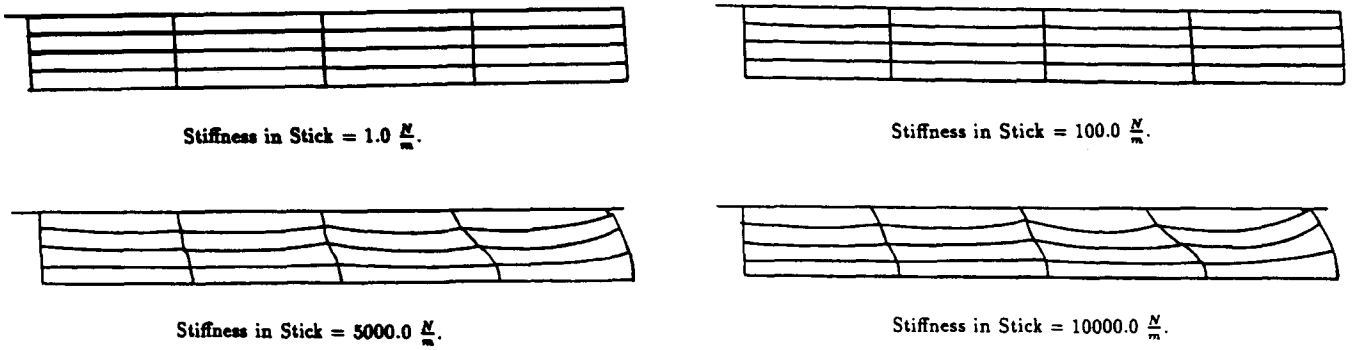

Fig. 2 Deformation pattern for stiffness in stick parameter.

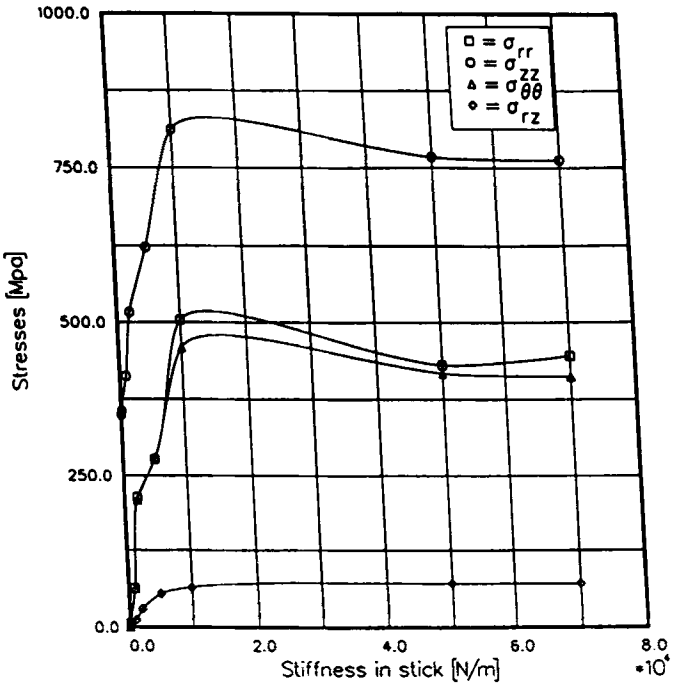

Fig. 3 Results of stiffness in stick study.

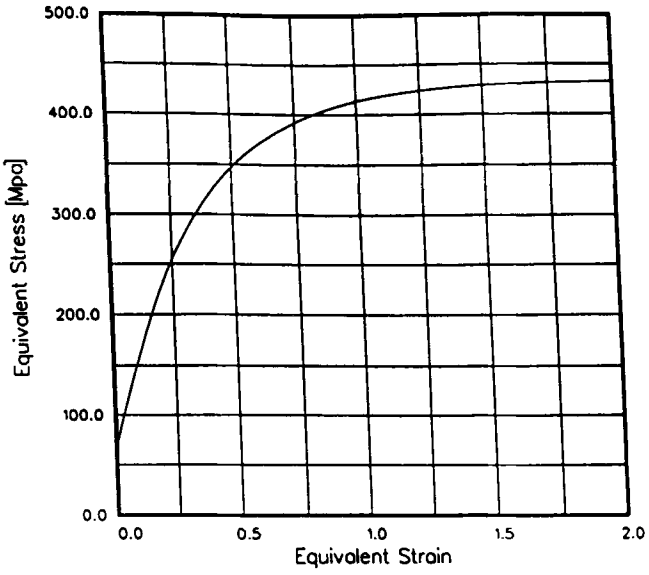

Fig. 4 Flow curve for OFHC copper.

ues of the component stresses and the equivalent stress are plotted versus the stiffness in stick parameter. Table 1 gives the maximum values of the component stresses, equivalent stress, and load for each compression simulation. The value used for the stiffness in stick does not affect the equivalent stress, because the saturation stress has been reached on the flow curve.

The component stress increases as the stiffness in stick increases, until the stiffness in stick reaches a value of 10,000 N/m. When the stiffness in stick is greater than 10,000 N/m, the component stress varies only slightly, and the deformation patterns are the same. At a stiffness in stick value of 80,000 N/m, the solution fails to converge. When large values of the stiffness in stick are used in the tube drawing process, the results follow the same trends as the compression tests; therefore, the largest value of the stiffness in stick that would provide coverage for all geometries of the tube drawing process is used in the tube drawing simulation.

The results of this study agree with the literature,[4] which suggests a very large value for the stiffness in stick, to approximate the process more accurately. A stiffness in stick value of 10^8 N/m was used for the tube drawing simulation. This is the highest value of the stiffness in stick that would converge at a solution for all geometries in the tube drawing process.

The material used in the simulation of the tube drawing process was OFHC copper. For cold forming, the effect of the strain rate is negligible, and the effect of the yield stress is most important.[5] The flow curve (Fig. 4) relating equivalent true stress and equivalent plastic strain is given by a saturation-type equation proposed by Voce:[6]

$$\bar{\sigma} = \sigma_s - (\sigma_s - \sigma_m) \exp\left[\left(\frac{-\sigma_m \varepsilon_m}{\sigma_s - \sigma_m}\right)\left(\frac{\bar{\varepsilon}}{\varepsilon_m} - 1\right)\right] \quad [15]$$

Table 2 Properties of OFHC Copper

Saturation stress (σ_s), MPa	433.35
Stress at maximum load (σ_m), MPa	322.10
Strain at maximum load (ε_m), ?	0.415
Modulus of elasticity (E), GPa	119.9
Poisson's ratio	0.322
Density, kg/m^3	8941.0
Thermal expansion, K^{-1}	17.6×10^{-6}
Thermal conductivity, W/m · K	394.5
Specific heat, J/kg · K	385.2
Inelastic heat friction	0.905
D, 1/sec	330.0
p	5

where σ_s is the saturation stress and σ_m and ε_m are the stress and strain at maximum load, respectively. The Voce saturation equation is the best fit curve for an elastic-plastic material.[7] The strain rate dependence is defined as:

$$\dot{\varepsilon}^{pl} = D\left(\frac{\sigma_e}{\sigma_o} - 1\right)^p \quad [16]$$

where $\dot{\varepsilon}^{pl}$ is the equivalent plastic strain, σ_e is the equivalent stress, σ_o is the yield stress, and D and p are material parameters. Table 2 gives the properties of OFHC copper used in the simulation. The inelastic heat friction is defined as the fraction of the rate of inelastic dissipation that appears as a heat source in the coupled temperature-displacement analysis.

For the Riks case, pressure is applied to the backside of the first radial row of elements entering the die and plug. The magnitude of the pressure is calculated by Riks analysis, as part of the solution. Riks analysis is set so that, when the last radial row of elements in the tube clears the die and plug, the analysis is stopped. For the coupled-displacement analysis, a displace-

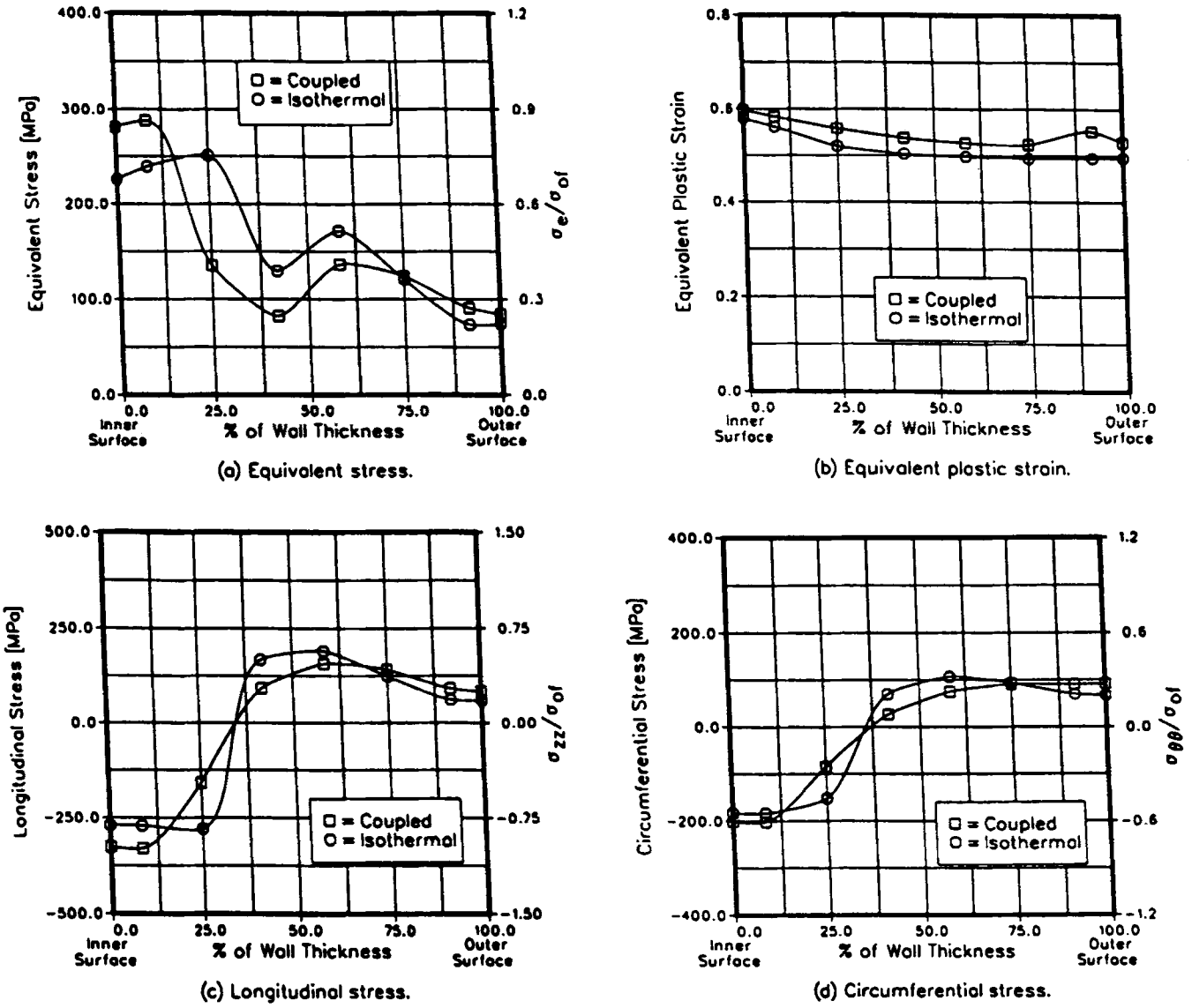

Fig. 5 Isothermal and coupled data at 10.9% reduction in area ($\alpha = 15.0$, $\beta = 7.5$).

ment is specified for the first radial row of elements entering the die and plug. This displacement is such that the entire workpiece is drawn through the die and plug.

4. Results and Discussion

The thermal effects on the tube drawing process were investigated for reductions in area of 10.9 and 37.1%. The die angle investigated was 15° and the plug angle was 7.5°. In Fig. 5 and 6, the equivalent stress, equivalent plastic strain, longitudinal residual stress, and circumferential residual stress are plotted against the percentage of wall thickness for the isothermal and coupled cases. The radial residual stress and the shear residual stress are not plotted, because their magnitudes are small compared to the longitudinal and circumferential residual stresses.

In the isothermal case, the Riks analysis was used. Using this method, pressure was applied to the back of the first radial row of elements, and the magnitude of the pressure was as large as the convergence rate would allow. The speed at which the tube was pulled through the die and plug was not controlled. In the coupled temperature-displacement analysis, a final displacement was specified for the first radial row of elements, and a number of small iterations was used to reach this displacement. The speed at which the tube was drawn through the die and plug was kept constant at 0.76 m/sec (2.5 ft/sec). In the coupled temperature-displacement analysis, the first radial row of elements was not allowed to deform freely. This was due to a constant displacement of the first radial row of nodes in the axial direction. This was compensated for by making the tube longer.

For the 10.9% reduction in area, the temperature increase was found to be 6.62 °C. In Fig. 5(b), the equivalent plastic

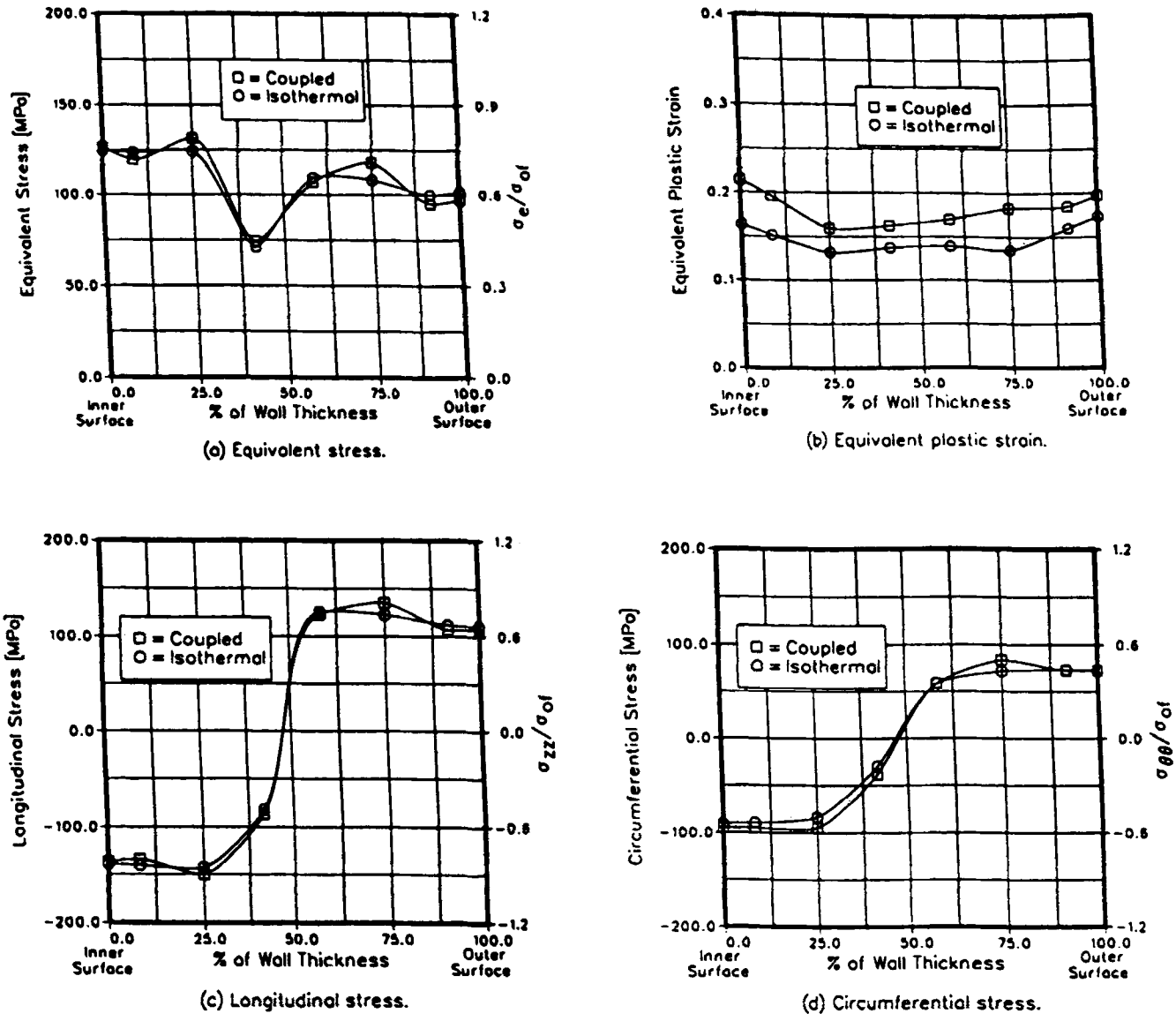

Fig. 6 Isothermal and coupled data at 37.1% reduction ($\alpha = 15.0$, $\beta = 7.5$).

Table 3 Effect of Drawing Speed on Temperature Increase

Drawing speed, m/sec	Temperature increase, °C
0.76	36.6
5.00	45.9
10.00	50.6
15.00	53.3
55.50	55.5

strain was slightly larger for the coupled case than for the isothermal case, due to the increase in temperature. The equivalent residual stress (Fig. 5a), longitudinal residual stress (Fig. 7c), and circumferential residual stress (Fig. 7d) were similar in the isothermal and coupled cases.

At 37.1% area reduction, the average temperature increase was 35.54 °C, and the maximum temperature increase was 36.63 °C. The maximum temperature increase occurred at the first radial row of elements and was due to the end effects. The temperature distribution was uniform away from the end effects. In Fig. 6(a), the equivalent plastic strain was slightly larger for the coupled case than for the isothermal case. However, the equivalent stress (Fig. 6b), longitudinal residual stress (Fig. 6c), and circumferential residual stress (Fig. 6d) were similar in the isothermal and coupled cases.

The effect of drawing speed on the temperature increase is summarized in Table 3 for an area reduction of 37.1%. The die and plug angles used were 15.0 and 7.5°, respectively. The most common speed used in tube drawing is 0.76 m/sec; however, tube can be drawn up to speeds of 20.0 m/sec. The coupled case was considered to be adiabatic, or no heat transferred from the tube. The boundary conditions were used to maximize the thermal effects on the tube. The temperature gradients over the cross section of the tube lead to different expansions and result in residual stresses.

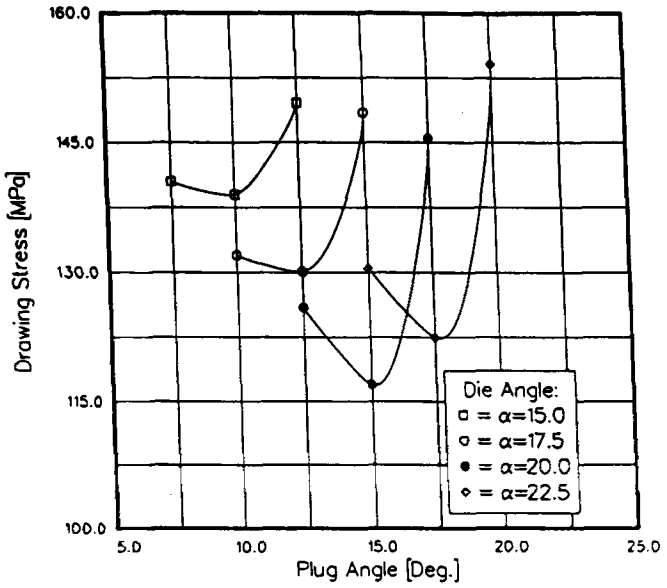

Fig. 7 Effect of plug angles on drawing stress at 10.9% reduction.

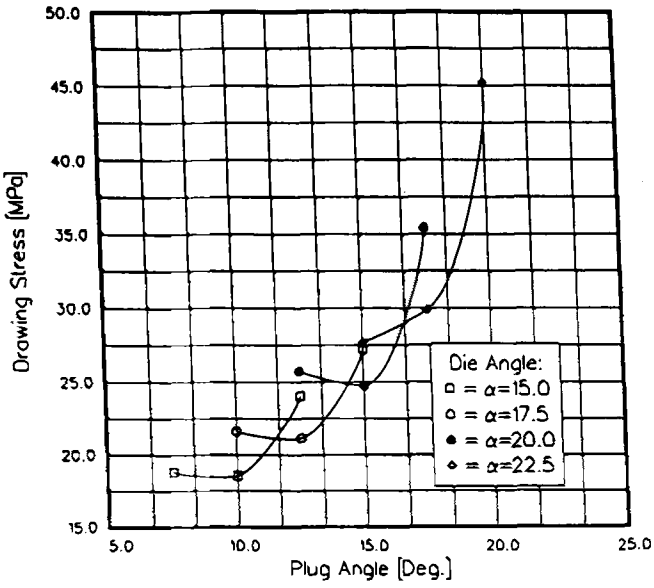

Fig. 8 Effect of plug angles on drawing stress at 37.1% reduction.

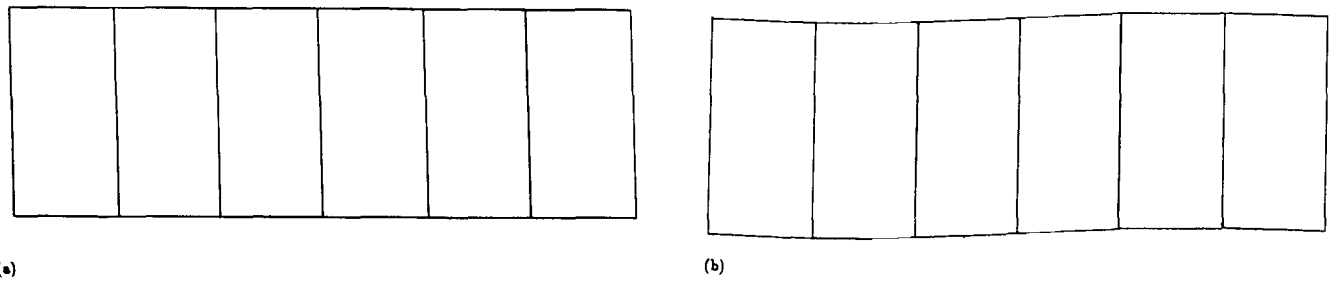

Fig. 9 Deformation patterns. **(a)** Undeformed radial row of elements. **(b)** Deformed radial row of elements.

The effect of various die and plug angles on the drawing stress was investigated at area reductions of 10.9 and 37.1%. The die angles investigated were 15.0, 17.5, 20.0, and 22.5°. The plug angles investigated were 10.0, 12.5, 15.0, and 17.5°. The effect of the plug angle at various die angles is shown in Fig. 7 for 10.9% area reduction and in Fig. 8 for 37.1% area reduction.

The optimum plug angle for 10.9% area reduction was 10.0°. As shown in Fig. 7, the optimum plug angle for each die angle was consistently 5.0° less than the die angle. The exception to this occurred at a die angle of 22.5° and an area reduction of 10.9%. This was possible due to the short length of the die and plug surfaces, caused by the small area reduction and large die angle.

The optimum plug angle for the 37.1% area reduction was 15.0°, as shown in Fig. 8. The above results are in excellent agreement with an earlier study by Hartley *et al.*[8] who used the upper bound approach to arrive at a similar conclusion regarding the existence of an optimum plug and die angle combination for the tube drawing process. Rees [1977] experimentally found the optimum die angle to be 18.0°, and the optimum plug angle to be 14.0°. From Fig. 7 and 8, the optimum plug angle for each die angle was consistently 5.0° less than the die angle.

The drawing stress required to overcome the die friction was high at low die angles, due to the length of the die. The frictional force was reduced as the die angle became greater, and the length of the die was shortened. As the die angle increases, the increased redundant work results in an increase in the drawing stress. Similarly, the optimum plug angle was a compromise between increased frictional resistance at plug angles close to the die angle and increased redundant work at a greater difference between the die angle and plug angle. The effect of increasing the area reduction was a shift in the optimum angles to higher values, due to the increasing frictional resistance as well as redundant work.

The effect of the die and plug angles on the residual stresses was investigated at die angles of 15.0, 17.5, 20.0, and 22.5° and at plug angles of 10.0, 12.5, 15.0, and 17.5°. The nonuniform deformation in the drawn tube resulted in a state of residual

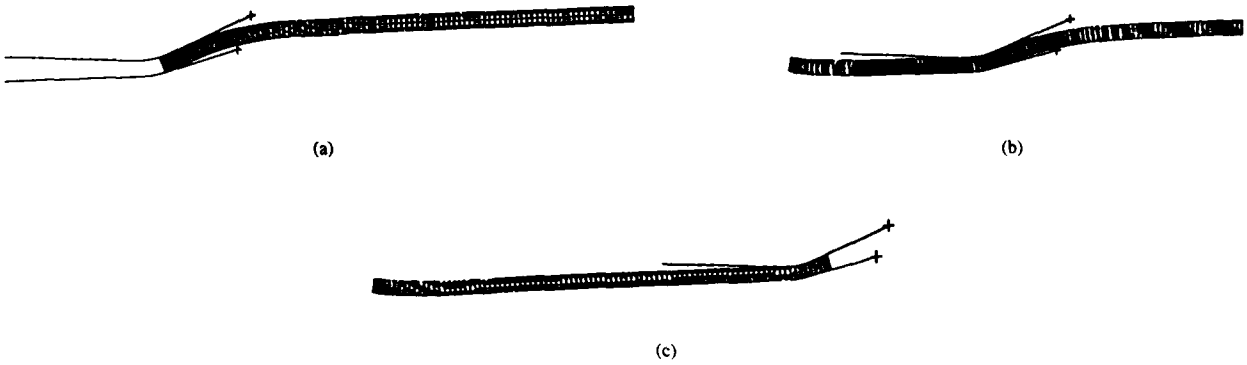

Fig. 10 Stages of tube drawing simulation. (**a**) First stage. (**b**) Second stage. (**c**) Third stage.

stress. Figure 9(a) shows one radial row of undeformed elements in the cross section of the tube. In Fig. 9(b), the radial row of elements has been deformed by the tube drawing process. Figure 10 shows the different stages of the tube drawing simulation.

Because there are no external forces acting on the tube after the tube drawing process is completed, the resultant longitudinal and circumferential forces, due to the residual stress acting on the cross section, must be zero. The magnitudes of the compressive and tensile longitudinal forces were within 2% of each other. The magnitudes of the compressive and tensile circumferential forces were within 4% of each other.

5. Conclusions and Recommendations

Thermal effects of slow speed tube drawing have minimal effect on the magnitude or distribution of the residual stresses. Good results for drawing stress and residual stresses are obtained with the finite-element method, assuming an isotropic material and constant friction at the die and plug interfaces. An optimum plug angle exists for each die angle, as well as an optimum die angle for each plug angle at each area reduction, for which the drawing stress is a minimum. The optimum die angles are 20.0 and 15.0°, and the optimum plug angles are 15.0 and 10.0° at area reductions of 10.9 and 37.1%, respectively. The friction losses are high for small die angles and for plug angles close to the die angle. Redundant work is high for large die angles and for plug angles further from the die angle. Residual stresses can be minimized by the proper selection of die and plug angles.

References

1. D.S. Chapman, "Effect of Process Variables on the Tube Drawing Process and Product Integrity," thesis, Texas Tech University, Lubbock, TX (1991).
2. H.D. Hibbit, Karlsson, and Sorenson, "ABAQUS Theory Manual," Version 4.7, Hibbit Karlsson and Sorenson Inc., Providence, RI (1989).
3. R. Kopp and M.L. Cho, "Influences of the Boundary Conditions on Results of the Finite-Element-Simulations," Proc. Second Int. Conf. Technology of Plasticity, Vol 1, Stuttgart, Germany, 43-50 (1987).
4. H.D. Hibbit, Karlsson, and Sorenson, "ABAQUS Users Manual," Version 4.7, Hibbit Karlsson and Sorenson Inc., Providence, RI (1989).
5. T. Altan and F.W. Boulger, "Flow Stress of Metal and Its Application in Metal Forming Analysis," *J. Eng. Ind.*, Nov, 1009-1019 (1973).
6. E. Voce, "The Relationship Between Stress and Strain for Homogeneous Deformation," *Int. Inst. Met.*, *74*, 537 (1948).
7. C.S. Hartley and R. Srinivasan, "Constitutive Equations for Large Plastic Deformations of Metals," *J. Eng. Mater. Technol.*, *105*, July, 162-167 (1983).
8. C.S. Hartley, "Optimum Processing Parameters for Floating Plug Tube Drawing," Proc. NAMRC VI, Society of Manufacturing Engineers, Apr 16-19, 193-198 (1978).

O.C. Zienkiewicz, E. Onate, and J.C. Heinrich, "A General Formulation for Coupled Thermal Flow of Metals Using Finite Element," *Int. J. Numerical Methods Eng.*, *1*, 75-100 (1981).

H.D. Hibbit, Karlsson, and Sorenson, "ABAQUS Example Problems Manual," Version 4.7, Hibbit Karlsson and Sorenson Inc., Providence, RI (1989).

the Finite-Element Simulations," Proceeding, Second International Conference on Technology of Plasticity, Stuttgart, Germany, Vol. 1, pp. 43-50